# Alignments in the odd-proton actinides $^{237}$Np and $^{241}$Am

K. Abu Saleem,[1,2] R. V. F. Janssens,[1] M. P. Carpenter,[1] F. G. Kondev,[1] I. Wiedenhöver,[1,3] I. Ahmad,[1] J. Caggiano,[1,*] P. Chowdhury,[4] J. A. Cizewski,[5] D. Cline,[6] M. Devlin,[7] N. Fotiades,[7] J. P. Greene,[1] G. Hackman,[8,*] A. Heinz,[1,†] T. L. Khoo,[1] T. Lauritsen,[1] C. J. Lister,[1] A. O. Macchiavelli,[9] E. H. Seabury,[7,‡] D. Seweryniak,[1] A. Sonzogni,[1,§] and C. Y. Wu[6]

[1]*Argonne National Laboratory, Argonne, Illinois 60439, USA*

[2]*Department of Physics, Illinois Institute of Technology, Chicago, Illinois 60616, USA*

[3]*Department of Physics, Florida State University, Tallahassee, Florida 32306, USA*

[4]*University of Massachusetts Lowell, Lowell, Massachusetts 01854, USA*

[5]*Department of Physics and Astronomy, Rutgers University, New Brunswick, New Jersey 08903, USA*

[6]*University of Rochester, Rochester, New York 14627, USA*

[7]*Los Alamos National Laboratory, Los Alamos, New Mexico 87545, USA*

[8]*University of Kansas, Lawrence, Kansas 66045-7582, USA*

[9]*Lawrence Berkeley National Laboratory, Berkeley, California 94720, USA*

(Received 18 May 2004; published 26 August 2004)

High spin states in $^{237}$Np and $^{241}$Am have been studied with the "unsafe" Coulomb excitation technique. In each nucleus, signature partner rotational bands built on the $[523]5/2^-$ and $[642]5/2^+$ orbitals of respective $h_{9/2}$ and $i_{13/2}$ parentage have been delineated. An additional pair of bands based on the $[521]3/2^-$ ($f_{7/2}$) state was also observed in $^{241}$Am. New information on the even-even $^{236}$Pu and $^{242}$Cm transfer products is also presented. From the present data, the role of $i_{13/2}$ protons in generating angular momentum in the even-even nuclei of the region is documented. A satisfactory description of the evolution of the rotational sequences with spin is achieved within the framework of the cranked shell model. Nevertheless, when combined with information on odd-neutron nuclei available from elsewhere, the data highlight significant shortcomings of the available theoretical predictions.

DOI: 10.1103/PhysRevC.70.024310 PACS number(s): 27.90.+b, 23.20.Lv, 21.10.Re, 21.60.Ev

## I. INTRODUCTION

Actinide nuclei are not only among the heaviest elements for which quantitative spectroscopic information can be obtained, they are also among the most deformed and, hence, the most collective nuclei available for experimental investigations. New studies of nuclei in this region have recently been undertaken for a number of reasons. First, questions remain regarding the alignment of $i_{13/2}$ protons and/or $j_{15/2}$ neutrons under the stress of rotation. In most yrast bands of the even-even actinides, a smooth gain in alignment with rotational frequency has been observed and the strong backbending phenomenon so often present in the rare earth nuclei is absent. This rise has been attributed to the successive alignments of pairs of $i_{13/2}$ protons and $j_{15/2}$ neutrons, although their respective contributions have not been delineated experimentally. In this context, the Pu isotopes have been calculated to be the exception rather than the rule as they are predicted to exhibit a strong backbending due to the $i_{13/2}$ proton alignment [1–3]. The calculations have been validated in $^{242,244}$Pu where a sudden gain in alignment first observed by Spreng *et al.* [1] has been fully delineated recently by Wiedenhöver *et al.* [4] and determined to be $10\hbar$, in agreement with theoretical expectations for a $i_{13/2}$ proton alignment. The alignment situation in the Pu isotopes is not entirely clear, however, since the sharp backbending observed in the heavier isotopes is not present within the same frequency range in the lighter $^{238,239,240}$Pu, implying at the minimum a significant delay in the alignment process [4]. There is at present no satisfactory explanation for these observations, although the presence of strong octupole correlations in the nuclei of interest has been proposed to play a significant role [4,5]. The nuclei $^{237}$Np and $^{241}$Am under study here are the two odd-proton systems closest to the Pu isotopes that are most readily accessible via Coulomb excitation. In both nuclei, the $i_{13/2}$ orbital lies close to the Fermi surface and the role of its alignment with frequency can be investigated by using Pauli blocking arguments in comparisons of the behavior of bands built on this $i_{13/2}$ state with those based on other excitations.

Another reason to investigate these nuclei further is that the *same* $j_{15/2}$ neutron and $i_{13/2}$ proton orbitals lie at the Fermi surface in the superdeformed nuclei of the $A\sim 190$ region [6]. Remarkably, most superdeformed nuclei of this region also exhibit a surprisingly smooth and gradual increase of their moments of inertia with frequency. In addition, there is a growing body of experimental data (spins, parities, excitation energies, $E1$ interband transition rates) [7,8] indicating strong octupole effects at large deformation. Thus, the opportunity exists to compare the impact of the intruder orbitals on nuclear structure in regimes corresponding to vastly different deformations. Finally, recent progress

*Present address: TRIUMF, Vancouver, BC, Canada V6T 2A3.

†Present address: WNSL, Yale University, New Haven, CT 06520-8124.

‡Present address: INEEL, Idaho Falls, ID 83415-3855.

§Present address: NNDC, Brookhaven National Laboratory, Upton, NY 11973-5000.

 

in experimental techniques has made the delineation of the yrast lines of nuclei with $Z > 100$ possible [9]. In these nuclei the evolution of the moments of inertia with frequency has also raised issues about, for example, the pairing strength or the location of specific orbitals with respect to the Fermi surface [10,11]. Studies of the nuclei closest in $A$ and $Z$ to the transfermium isotopes may be able to shed light on some of the same issues, while providing information on the types of excitations that can be expected along the yrast line and in its immediate vicinity.

As stated above, this paper explores the level structures of the long-lived actinide nuclei $^{237}$Np and $^{241}$Am. The experimental approach used follows the pioneering work of Ward *et al.* [12] who demonstrated the power of inelastic scattering at beam energies slightly above the Coulomb barrier on thick/backed targets as a means of studying collective excitations with high sensitivity. At these beam energies, the cross sections for feeding the highest spin states are enhanced, and events with a high $\gamma$-ray multiplicity select the longest rotational cascades (which involve the highest spin levels). Under such conditions, most of the $\gamma$ rays are emitted after the excited nucleus has come to rest, and the vast majority of transitions in a collective cascade are measured with the intrinsic resolution of the Ge detectors. This feature is especially useful in the actinide nuclei where many collective bands are characterized by nearly degenerate transition energies.

The present study is the first to investigate high spin properties in $^{241}$Am. Earlier decay and light-ion transfer measurements, summarized in Ref. [13], had established the low spin states on which the level scheme reported here is based. In addition to similar information on the lowest excited levels in $^{237}$Np [14], the investigation of this nucleus benefited from an earlier Coulomb excitation experiment by Kulessa *et al.* [15] where the yrast structure was delineated.

Experimental considerations as well as relevant details of the analysis techniques are briefly described in the next section (Sec. II). *A* presentation of the results on the two odd actinide nuclei under consideration can be found in Sec. III which also briefly discusses new data on the even neighboring nuclei $^{242}$Cm and $^{236}$Pu reached in the present study via transfer reactions. Section IV discusses comparisons between the experimental observations and cranked shell model (CSM) calculations. A brief summary and conclusions can be found in the last section.

## II. EXPERIMENTAL PROCEDURE AND DATA REDUCTION

Targets of the long-lived $^{237}$Np isotope ($t_{1/2} = 2.14 \times 10^6$ y, enrichment $\sim$99%) with a thickness of 300 $\mu$g/cm$^2$ were electroplated onto 50-mg/cm$^2$-thick Au foils. In addition, a second thin Au foil ($\sim$50 $\mu$g/cm$^2$) was mounted in front of each target to minimize the possibility of contaminating the experimental equipment by the release of radioactive target material. A description of the chemical purification of the material before deposition and of the molecular plating process itself can be found in Ref. [16]. Because $^{241}$Am is an $\alpha$ emitter with a half life of only 432.7 y, targets of this element were limited to a thickness of 110 $\mu$g/cm$^2$ corresponding to a measured activity of roughly 80 $\mu$Ci. In this case as well the targets (with an enrichment $\geqslant$99%) were electroplated on Au substrates and covered with a thin Au front layer.

$^{209}$Bi beams with an intensity of $\sim$1 *pnA* and an energy of 1450 MeV, i.e., $\sim$10–15% above the Coulomb barrier for the projectile-target combinations under consideration, were delivered by the ATLAS superconducting linear accelerator at Argonne National Laboratory. Gamma rays were detected with the Gammasphere array [17] which, in its configuration for experiments at ATLAS, comprises 101 Compton-suppressed Ge spectrometers. Events were written to tape when four or more suppressed Ge detectors fired in prompt coincidence. The total number of coincidence events written to tape during the one-day experiment with the $^{237}$Np target was $2.1 \times 10^8$. The corresponding number for $^{241}$Am was $5.3 \times 10^8$ events and these were collected in three days. In addition to the Ge information, the total multiplicity and sum energy measured by Gammasphere (measured in both the BGO suppressor shields and in the Ge detectors) was also written to tape event by event as the collimators, placed in front of the BGO shields for most applications, were not present for these measurements.

Most of the data analysis was based on coincidence $\gamma$-$\gamma$-$\gamma$ cubes constructed under a number of conditions. As stated above, cubes properly gated on total multiplicity and sum energy were used to select the longest $\gamma$-ray cascades [12]. In addition, a number of cubes gated on known yrast transitions in the nuclei of interest proved instrumental in uncovering the weakest members of the cascades as well as additional structures feeding the strongest bands. Finally, triple coincidence histograms were also obtained with gates placed either on the 896 keV ground state transition in $^{209}$Bi or on the two lowest lines (583 and 2614 keV) in $^{208}$Pb in order to confirm the association of the observed $\gamma$ rays with the excitation of the target or with the proton transfer channel. Proper subtraction of random coincidence events proved essential in order to remove the contamination of the spectra by the intense $\gamma$ rays from $^{197}$Au Coulomb excitation. The data analysis was performed with the programs of the RADWARE package [18]. Further details about the analysis can be found in Ref. [19].

## III. EXPERIMENTAL RESULTS

### A. $^{237}$Np

As stated above, previous work on this nucleus is summarized in Ref. [14]. The $^{237}$Np level scheme obtained in this work is presented in Fig. 1, and consists of four bands numbered from 1 to 4. Following Ref. [14], bands 1 and 2, the ground state signature partner bands, are built on the $[642]5/2^+$ configuration of $i_{13/2}$ parentage, while bands 3 and 4, the other pair of signature partners, are built on the $[523]5/2^-$ configuration which originates from the $h_{9/2}$ state. The transitions placed in the level scheme are given in Table I together with level energies and spin assignments [20].

A representative coincidence spectrum for bands 1 and 2 is given in Fig. 2. The spectrum is a sum of all double coin-

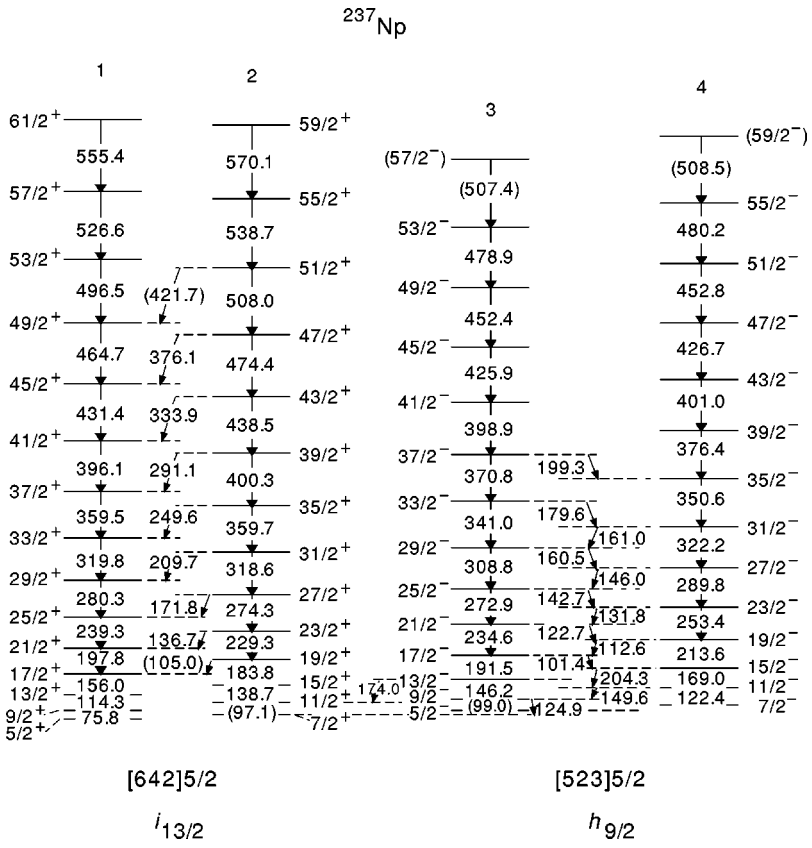


FIG. 1. Proposed level scheme for $^{237}$Np; the energies of the transitions are given in keV. States and $\gamma$ rays for which the placement should be viewed as tentative are given in parentheses.

cidence gates placed on the 197.8–396.1 keV sequence. Besides the expected $\gamma$ rays assigned to the two bands and the Np x rays, the spectrum also displays the 896 keV line resulting from the excitation of the $^{209}$Bi projectile. The observation of this particular transition in coincidence confirms that the $\gamma$ rays under investigation are associated with the inelastic excitation channel. Band 1 was found to consist of 14 in-band transitions, i.e., one additional transition has been placed at the top of the sequence with respect to the work of Ref. [15]. In comparison to the latter work, only the 43 keV, $9/2^+ \rightarrow 7/2^+$ transition towards band 2 was not observed here because of the lack of efficiency of the Gammasphere at this low energy and the large contribution of the internal conversion process to the deexcitation. Similarly, band 2 was also extended by one new $\gamma$ ray and now consists of 13 in-band and nine out-of-band transitions. The out-of-band lines link the $(2I+1)^+/2$ levels with the $(2I-1)^+/2$ states in band 1, and are thus of mixed $M1/E2$ character. The 33 and 54 keV $\gamma$ rays assigned to the $7/2^+ \rightarrow 5/2^+$ and $11/2^+ \rightarrow 9/2^+$ transitions, respectively, could not be observed because of their low energy. It is worth noting that most of the transition energies in these two bands differ by $\sim$1 keV from those of Ref. [15]. Confidence in the energies of Table I comes from the careful calibration of Gammasphere with radioactive sources and from further checks with known transitions measured in-beam (from the Au backing and transitions in strong reaction channels).

The data collected in the present work have significantly extended the available information on bands 3 and 4 as compared to the most recent compilation [14]. These bands were fed in the present measurement with an intensity of $\sim$50% that measured for bands 1 and 2. The bands now extend to the $57/2^-$ and $59/2^-$ states with excitation energies of 4.29 and 4.47 MeV, respectively. As can be seen in Fig. 1, eight out-of-band $\gamma$ rays have been placed draining $\gamma$-ray intensity out of band 3. The out-of-band 124.9 and 174.0 keV transitions were found to feed the $7/2^+$ and $11/2^+$ levels in band 2, while the other out-of-band $\gamma$ rays link the $(2I+1)^-/2$ states with the $(2I-1)^-/2$ levels in band 4. The ordering of $\gamma$ rays in the cascade relies on the observed coincidence relationships and on the relative intensities of the transitions. Thirteen in-band $\gamma$ rays could be placed in band 4. In addition, a four-transition branch linking the $(2I+1)^-/2$ states with $(2I-1)^-/2$ levels in band 3 was established as well. Finally, a link with band 1 has been found as the 149.6 and 204.3 keV $\gamma$ rays were shown to feed the $9/2^+$ and $13/2^+$ states. Placing a double coincidence gate on transitions at the bottom of the band reveals the $\gamma$ rays in the cascade with a decreasing intensity as the spin increases. In addition, most of the lines in band 3 can be seen as well because of the transitions linking the two sequences. As an example, Fig. 3 shows the $\gamma$ rays of bands 3 and 4 as well as the characteristic Np x rays from a coincidence spectrum requiring the presence of at least one transition of the sequence 213.6–376.4 keV and another from the 401.0–480.2 keV cascade.

### B. $^{241}$Am

The present work represents the first high spin study of $^{241}$Am. The compilation of Ref. [13] served as the starting point for the development of the level scheme presented in Fig. 4. This scheme now comprises six rotational bands with

TABLE I. Level excitation energies and spins, as well as transition energies and placements for $^{237}$Np; the uncertainties on the transition energies are 0.2 keV for the strongest transitions and 0.5 keV for the weakest. Transitions in parentheses were seen clearly only in sums of gated coincidence spectra.

| $E_x$ (keV) | $J^\pi$ ($\hbar$) | $E_\gamma$ (keV) | Assignment | $E_x$ (keV) | $J^\pi$ ($\hbar$) | $E_\gamma$ (keV) | Assignment |
|---|---|---|---|---|---|---|---|
| | | Band 1 | | | | Band 2 | |
| 0.0 | $5/2^+$ | | | | | | |
| 75.8 | $9/2^+$ | 75.8 | $9/2^+ \rightarrow 5/2^+$ | 33.2 | $7/2^+$ | | |
| 190.1 | $13/2^+$ | 114.3 | $13/2^+ \rightarrow 9/2^+$ | 130.3 | $11/2^+$ | (97.1) | $11/2^+ \rightarrow 7/2^+$ |
| 346.1 | $17/2^+$ | 156.0 | $17/2^+ \rightarrow 13/2^+$ | 269.0 | $15/2^+$ | 138.7 | $15/2^+ \rightarrow 11/2^+$ |
| 543.9 | $21/2^+$ | 197.8 | $21/2^+ \rightarrow 17/2^+$ | 452.8 | $19/2^+$ | 183.8 | $19/2^+ \rightarrow 15/2^+$ |
| | | | | | | (105.0) | $19/2^+ \rightarrow 17/2^+$ |
| 783.2 | $25/2^+$ | 239.3 | $25/2^+ \rightarrow 21/2^+$ | 682.1 | $23/2^+$ | 229.3 | $23/2^+ \rightarrow 19/2^+$ |
| | | | | | | 136.7 | $23/2^+ \rightarrow 21/2^+$ |
| 1063.5 | $29/2^+$ | 280.3 | $29/2^+ \rightarrow 25/2^+$ | 956.4 | $27/2^+$ | 274.3 | $27/2^+ \rightarrow 23/2^+$ |
| | | | | | | 171.8 | $27/2^+ \rightarrow 25/2^+$ |
| 1383.3 | $33/2^+$ | 319.8 | $33/2^+ \rightarrow 29/2^+$ | 1275.0 | $31/2^+$ | 318.6 | $31/2^+ \rightarrow 27/2^+$ |
| | | | | | | 209.7 | $31/2^+ \rightarrow 29/2^+$ |
| 1742.8 | $37/2^+$ | 359.5 | $37/2^+ \rightarrow 33/2^+$ | 1634.7 | $35/2^+$ | 359.7 | $35/2^+ \rightarrow 31/2^+$ |
| | | | | | | 249.6 | $35/2^+ \rightarrow 33/2^+$ |
| 2138.9 | $41/2^+$ | 396.1 | $41/2^+ \rightarrow 37/2^+$ | 2035.0 | $39/2^+$ | 400.3 | $39/2^+ \rightarrow 35/2^+$ |
| | | | | | | 291.1 | $39/2^+ \rightarrow 37/2^+$ |
| 2570.3 | $45/2^+$ | 431.4 | $45/2^+ \rightarrow 41/2^+$ | 2473.5 | $43/2^+$ | 438.5 | $43/2^+ \rightarrow 39/2^+$ |
| | | | | | | 333.9 | $43/2^+ \rightarrow 41/2^+$ |
| 3035.0 | $49/2^+$ | 464.7 | $49/2^+ \rightarrow 45/2^+$ | 2947.9 | $47/2^+$ | 474.4 | $47/2^+ \rightarrow 43/2^+$ |
| | | | | | | 376.1 | $47/2^+ \rightarrow 45/2^+$ |
| 3531.5 | $53/2^+$ | 496.5 | $53/2^+ \rightarrow 49/2^+$ | 3455.9 | $51/2^+$ | 508.0 | $51/2^+ \rightarrow 47/2^+$ |
| | | | | | | (421.7) | $51/2^+ \rightarrow 49/2^+$ |
| 4058.1 | $57/2^+$ | 526.6 | $57/2^+ \rightarrow 53/2^+$ | 3994.6 | $55/2^+$ | 538.7 | $55/2^+ \rightarrow 51/2^+$ |
| 4613.5 | $61/2^+$ | 555.4 | $61/2^+ \rightarrow 57/2^+$ | 4564.7 | $59/2^+$ | 570.1 | $59/2^+ \rightarrow 55/2^+$ |
| | | Band 3 | | | | Band 4 | |
| 59.1 | $5/2^-$ | | | 103.0 | $7/2^-$ | | |
| 158.1 | $9/2^-$ | (99.0) | $9/2^- \rightarrow 5/2^-$ | 225.4 | $11/2^-$ | 122.4 | $11/2^- \rightarrow 7/2^-$ |
| | | 124.9 | $9/2^- \rightarrow 7/2^+$ | | | 149.6 | $11/2^- \rightarrow 9/2^+$ |
| 304.3 | $13/2^-$ | 146.2 | $13/2^- \rightarrow 9/2^-$ | 394.4 | $15/2^-$ | 169.0 | $15/2^- \rightarrow 11/2^-$ |
| | | 174.0 | $13/2^- \rightarrow 11/2^+$ | | | 204.3 | $15/2^- \rightarrow 13/2^+$ |
| 495.8 | $17/2^-$ | 191.5 | $17/2^- \rightarrow 13/2^-$ | 608.0 | $19/2^-$ | 213.6 | $19/2^- \rightarrow 15/2^-$ |
| | | 101.4 | $17/2^- \rightarrow 15/2^-$ | | | 112.6 | $19/2^- \rightarrow 17/2^-$ |
| 730.4 | $21/2^-$ | 234.6 | $21/2^- \rightarrow 17/2^-$ | 861.4 | $23/2^-$ | 253.4 | $23/2^- \rightarrow 19/2^-$ |
| | | 122.7 | $21/2^- \rightarrow 19/2^-$ | | | 131.8 | $23/2^- \rightarrow 21/2^-$ |
| 1003.3 | $25/2^-$ | 272.9 | $25/2^- \rightarrow 21/2^-$ | 1151.2 | $27/2^-$ | 289.8 | $27/2^- \rightarrow 23/2^-$ |
| | | 142.7 | $25/2^- \rightarrow 23/2^-$ | | | 146.0 | $27/2^- \rightarrow 25/2^-$ |
| 1312.1 | $29/2^-$ | 308.8 | $29/2^- \rightarrow 25/2^-$ | 1473.4 | $31/2^-$ | 322.2 | $31/2^- \rightarrow 27/2^-$ |
| | | 160.5 | $29/2^- \rightarrow 27/2^-$ | | | 161.0 | $31/2^- \rightarrow 29/2^-$ |
| 1653.1 | $33/2^-$ | 341.0 | $33/2^- \rightarrow 29/2^-$ | 1824.0 | $35/2^-$ | 350.6 | $35/2^- \rightarrow 31/2^-$ |
| | | 179.6 | $33/2^- \rightarrow 31/2^-$ | | | | |
| 2023.9 | $37/2^-$ | 370.8 | $37/2^- \rightarrow 33/2^-$ | 2200.4 | $39/2^-$ | 376.4 | $39/2^- \rightarrow 35/2^-$ |
| | | 199.3 | $37/2^- \rightarrow 35/2^-$ | | | | |
| 2422.8 | $41/2^-$ | 398.9 | $41/2^- \rightarrow 37/2^-$ | 2601.4 | $43/2^-$ | 401.0 | $43/2^- \rightarrow 39/2^-$ |
| 2848.7 | $45/2^-$ | 425.9 | $45/2^- \rightarrow 41/2^-$ | 3028.1 | $47/2^-$ | 426.7 | $47/2^- \rightarrow 43/2^-$ |

TABLE I. (*Continued.*)

| $E_x$ (keV) | $J^\pi$ ($\hbar$) | $E_\gamma$ (keV) | Assignment | $E_x$ (keV) | $J^\pi$ ($\hbar$) | $E_\gamma$ (keV) | Assignment |
|---|---|---|---|---|---|---|---|
| Band 3 | | | | Band 4 | | | |
| 3301.1 | $49/2^-$ | 452.4 | $49/2^- \rightarrow 45/2^-$ | 3480.9 | $51/2^-$ | 452.8 | $51/2^- \rightarrow 47/2^-$ |
| 3780.0 | $53/2^-$ | 478.9 | $53/2^- \rightarrow 49/2^-$ | 3961.1 | $55/2^-$ | 480.2 | $55/2^- \rightarrow 51/2^-$ |
| 4287.4 | $(57/2^-)$ | (507.4) | $(57/2^-) \rightarrow 53/2^-$ | 4469.6 | $(59/2^-)$ | (508.5) | $(59/2^-) \rightarrow 55/2^-$ |

a total of 123 transitions. The relevant level energies, spin assignments and transition placements are given in Table II. Bands 1 and 2 are the signature partners of the ground state band built on the $[523]5/2^-$ state of $h_{9/2}$ parentage [13]. The signature partner bands 3 and 4 are built on the $[642]5/2^+$ configuration originating from the $i_{13/2}$ intruder orbital, while the signature partner bands 5 and 6 are built on the $[521]3/2^-$ state with $2f_{7/2}$ parentage. Note the reverse ordering of the parent orbitals for bands 1 and 2 vs 3 and 4 with respect to their counterparts in $^{237}$Np.

Prior to the present study, only the states with spin $5/2^- - 13/2^-$ in bands 1 and 2 had been proposed [13]. The two sequences are now firmly established on the basis of the observed coincidence relationships up to $65/2^-$ in band 1 and $63/2^-$ in band 2 (Fig. 4). Up to moderate spin ($I \sim 41/2$), the two sequences are also linked by transitions of mixed $M1/E2$ character and, as a result, a coincidence spectrum gated on low spin transitions in one signature partner also shows in-band transitions from the other. This is illustrated in Fig. 5, where a coincidence spectrum produced as a sum of clean double gates in the 139.9–378.0 keV sequence of band 1 displays members of both bands. The tentative placement of the 573.0 keV transition at the top of band 1 results from the observation of a weak transition at this energy in sums of coincidence spectra double gated on transitions between high spin levels in the cascade. This approach selects the events with the highest multiplicity and, thus, enhances the decay of the highest spin states (the procedure is illustrated graphically below in the case of band 4).

The next strongest structure in $^{241}$Am (with roughly half the intensity of bands 1 and 2), the signature partner bands 3 and 4 (Fig. 4), is based on the $[642]5/2^+$ configuration of $i_{13/2}$ parentage for which only the $5/2^+$ bandhead had been firmly established previously, although candidate levels with spin 7/2, 9/2, 11/2 and 13/2 had also been tentatively assigned [13]. Band 3 has been established to the $69/2^+$ level at an excitation energy of 5.82 MeV, and the signature partner, band 4, has now been delineated up to the $59/2^+$ state at an excitation energy of 4.58 MeV. In addition, linking transitions with the ground state band have been observed so that all excitation energies are firm. Just as in the case of bands 1 and 2, $\gamma$ rays linking some of the alternate levels in the two signature partner bands have also been observed, although with weaker intensity than in the ground state sequence. Band 3 consists of 26 in- and out-of-band $\gamma$ rays. All the in-band transitions from the $65/2^+$ level to the $5/2^+$ bandhead have been directly observed in individual coincidence spectra with the exception of the low energy $9/2^+ \rightarrow 5/2^+$ line. Similarly, all of the in-band $\gamma$ rays in band 4 have been directly observed, except the low energy $11/2^+ \rightarrow 7/2^+$ transition. Note that the $\gamma$ rays of band 3 are rather close in energy to those in band 4. In particular, the $41/2^+ \rightarrow 37/2^+$ transition (386.2 keV) is almost identical to the $39/2^+ \rightarrow 35/2^+$ deexcitation (386.4 keV) in Band 4. Therefore, in

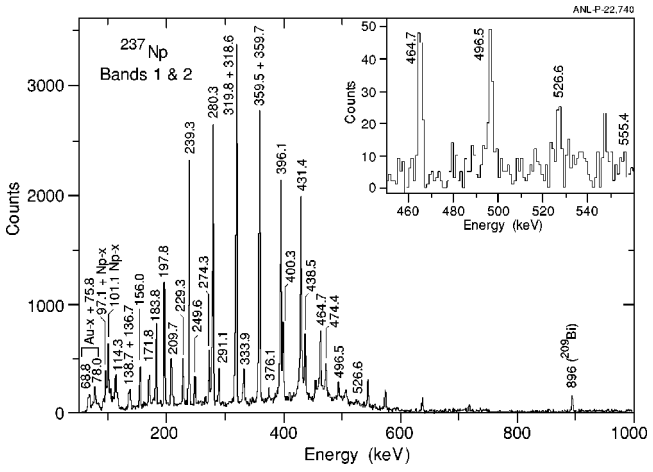


FIG. 2. Representative coincidence spectrum for the signature partner bands 1 and 2 in $^{237}$Np. The spectrum is the result of a sum of double coincidence gates placed on transitions in the 197.8–396.1 keV cascade. Note the presence of the 896 keV projectile excitation. Unmarked peaks in the spectrum correspond to identified contaminants which were not labeled for clarity.

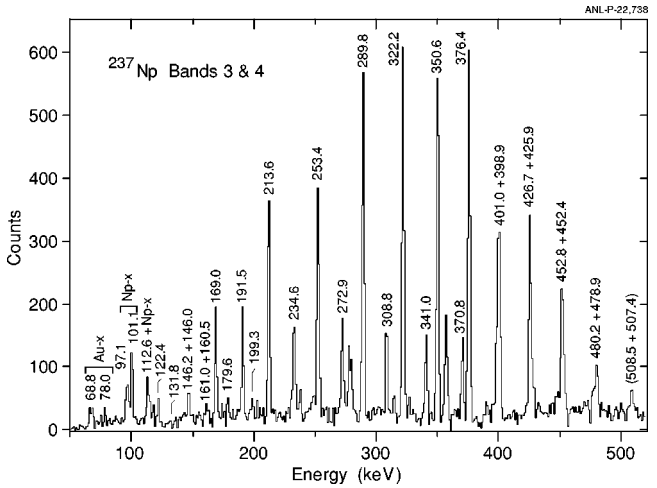


FIG. 3. Representative coincidence spectrum for bands 3 and 4 in $^{237}$Np. The spectrum is the result of a sum of double coincidence gates placed on one transition in the 213.6–376.4 keV cascade and on a $\gamma$ ray in the 401.0–480.2 keV sequence.

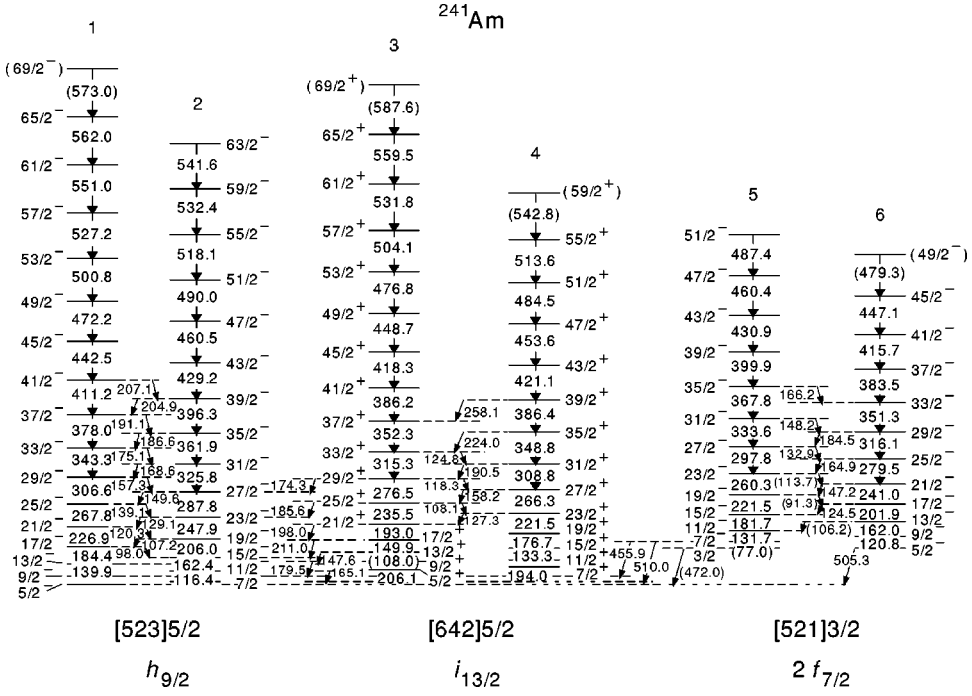


FIG. 4. Proposed level scheme for $^{241}$Am; the energies of the transitions are given in keV. States and $\gamma$ rays for which the placement should be viewed as tentative are given in parentheses.

order to ensure that the assignment of the $\gamma$ rays is correct, it was often important to gate both below and above a level to confirm the placements. The 504.1 keV $\gamma$ ray, corresponding to the $57/2^+ \rightarrow 53/2^+$ transition, is a good example. Figure 6 shows a representative spectrum. The large diagram in this figure is the result of a sum over double coincidence gates placed on the series 235.5–386.2 keV together with the 418.3–476.8 keV transitions. For the highest spin states, the deexciting 476.8, 531.8, 559.5, and 587.6 keV lines are best seen in a double coincidence gate placed on the 504.1 keV $\gamma$ ray together with the 386.2–476.8 keV series. The high energy part of the spectrum of interest is shown in the inset of Fig. 6. Just as was the case in band 1, the highest transition in bands 3 and 4 should be viewed as tentative since they have been obtained mostly from summed coincidence spectra.

Bands 5 and 6 in Fig. 4 are associated with the $[521]3/2^-$ configuration. These bands are present in the data with an intensity of 5–8% that of bands 1 and 2. Prior to this study, the $3/2^-$, $5/2^-$, and $7/2^-$ states, with respective excitation energies of 471.8, 504.4, and 549 keV, were known [13], and the 682 keV, $11/2^-$ level was tentatively assigned to this configuration. Here, this structure has been delineated up to the $51/2^-$ and $49/2^-$ states at excitation energies of 4.12 and 3.90 MeV for bands 5 and 6, respectively. In addition, linking transitions with the ground state band as well as $\gamma$ rays between the alternate levels have been discovered. As is expected in the case of strongly coupled bands, placing double coincidence gates on pairs of $\gamma$ rays at the bottom of one of the signature partner bands reveals the in-band transitions with decreasing intensity as a function of spin as well as the $\gamma$ rays of the signature partner band. Careful checking of all observed coincidence relationships validates the scheme of Fig. 4 in which the total number of transitions assigned to this configuration has been raised to 37.

### C. Results from other reaction channels: $^{236}$Pu and $^{242}$Cm

The beam energy used in the experiments is roughly 10–15% above the Coulomb barrier for the two projectile-target combinations under investigation and, as a result, reactions including the exchange of one or more nucleons have been observed as well. The cross sections for these processes are only a few percent of the "unsafe" Coulomb excitation channel [19], and the resolving power of the Gammasphere has proved essential in extracting data from the complex spectra. Here, results are presented only for the $^{242}$Cm and $^{236}$Pu nuclei where information was obtained in relation to the issue of delayed alignments raised originally in Ref. [4] and introduced above.

The most difficult case encountered was that of $^{242}$Cm, the nucleus reached via the one proton transfer reaction on the $^{241}$Am target. Prior to the present work, only the three lowest excited states of the ground state band were known from an $\alpha$ decay measurement [21] and the corresponding transition energies are: 42.1(±1) keV $(2^+ \rightarrow 0^+)$, 96(±3) keV $(4^+ \rightarrow 2^+)$ and 147(±5) keV $(6^+ \rightarrow 4^+)$. The 42 keV transition is too low in energy to be visible in Gammasphere data. In addition, the 96 keV line is in the target x-ray region of the spectrum and is essentially impossible to observe as well. With a coincidence gate placed on the Cm x rays, the region around 147 keV was carefully scanned in search of the $6^+ \rightarrow 4^+$ transition. A sequence of nine lines appeared in coincidence with a 150.2 keV $\gamma$ ray and the Cm x rays. The energy of this 150.2 keV transition is well within the uncertainty of the previous measurement. Furthermore, this sequence was also found to be in coincidence with the 2614 keV $3^- \rightarrow 0^+$ and the 583 keV, $5^- \rightarrow 3^-$ transitions in $^{208}$Pb, the partner of $^{242}$Cm in the one proton $^{241}$Am($^{209}$Bi, $^{208}$Pb)$^{242}$Cm transfer reaction. The results of this analysis are illustrated in Fig. 7,

TABLE II. Level excitation energies and spins, as well as transition energies and placements for $^{241}$Am; the uncertainties on the transition energies are 0.2 keV for the strongest transitions and 0.5 keV for the weakest. Transitions in parentheses were seen clearly only in sums of gated coincidence spectra.

| $E_x$ (keV) | $J^\pi$ ($\hbar$) | $E_\gamma$ (keV) | Assignment | $E_x$ (keV) | $J^\pi$ ($\hbar$) | $E_\gamma$ (keV) | Assignment |
|---|---|---|---|---|---|---|---|
| | | Band 1 | | | | Band 2 | |
| 0.0 | $5/2^-$ | | | 41.2 | $7/2^-$ | | |
| 93.7 | $9/2^-$ | | | 157.6 | $11/2^-$ | 116.4 | $11/2^- \rightarrow 9/2^-$ |
| 233.5 | $13/2^-$ | 139.9 | $13/2^- \rightarrow 9/2^-$ | 320.0 | $15/2^-$ | 162.4 | $15/2^- \rightarrow 11/2^-$ |
| 417.9 | $17/2^-$ | 184.4 | $17/2^- \rightarrow 13/2^-$ | 526.0 | $19/2^-$ | 206.0 | $19/2^- \rightarrow 15/2^-$ |
| | | 98.0 | $17/2^- \rightarrow 15/2^-$ | | | 107.2 | $19/2^- \rightarrow 17/2^-$ |
| 644.8 | $21/2^-$ | 226.9 | $21/2^- \rightarrow 17/2^-$ | 773.9 | $23/2^-$ | 247.9 | $23/2^- \rightarrow 19/2^-$ |
| | | 120.3 | $21/2^- \rightarrow 19/2^-$ | | | 129.1 | $23/2^- \rightarrow 21/2^-$ |
| 912.6 | $25/2^-$ | 267.8 | $25/2^- \rightarrow 21/2^-$ | 1061.7 | $27/2^-$ | 287.8 | $27/2^- \rightarrow 23/2^-$ |
| | | 139.1 | $25/2^- \rightarrow 23/2^-$ | | | 149.6 | $27/2^- \rightarrow 25/2^-$ |
| 1219.2 | $29/2^-$ | 306.6 | $29/2^- \rightarrow 25/2^-$ | 1387.5 | $31/2^-$ | 325.8 | $31/2^- \rightarrow 27/2^-$ |
| | | 157.3 | $29/2^- \rightarrow 27/2^-$ | | | 168.6 | $31/2^- \rightarrow 29/2^-$ |
| 1562.6 | $33/2^-$ | 343.3 | $33/2^- \rightarrow 29/2^-$ | 1749.4 | $35/2^-$ | 361.9 | $35/2^- \rightarrow 31/2^-$ |
| | | 175.1 | $33/2^- \rightarrow 31/2^-$ | | | 186.6 | $35/2^- \rightarrow 33/2^-$ |
| 1940.6 | $37/2^-$ | 378.0 | $37/2^- \rightarrow 33/2^-$ | 2145.7 | $39/2^-$ | 396.3 | $39/2^- \rightarrow 35/2^-$ |
| | | 191.1 | $37/2^- \rightarrow 35/2^-$ | | | 204.9 | $39/2^- \rightarrow 37/2^-$ |
| 2351.8 | $41/2^-$ | 411.2 | $41/2^- \rightarrow 37/2^-$ | 2574.9 | $43/2^-$ | 429.2 | $43/2^- \rightarrow 39/2^-$ |
| | | 207.1 | $41/2^- \rightarrow 39/2^-$ | | | | |
| 2794.2 | $45/2^-$ | 442.5 | $45/2^- \rightarrow 41/2^-$ | 3035.4 | $47/2^-$ | 460.5 | $47/2^- \rightarrow 43/2^-$ |
| 3266.4 | $49/2^-$ | 472.2 | $49/2^- \rightarrow 45/2^-$ | 3525.4 | $51/2^-$ | 490.0 | $51/2^- \rightarrow 47/2^-$ |
| 3767.2 | $53/2^-$ | 500.8 | $53/2^- \rightarrow 49/2^-$ | 4043.6 | $55/2^-$ | 518.1 | $55/2^- \rightarrow 51/2^-$ |
| 4294.5 | $57/2^-$ | 527.2 | $57/2^- \rightarrow 53/2^-$ | 4575.9 | $59/2^-$ | 532.4 | $59/2^- \rightarrow 55/2^-$ |
| 4845.5 | $61/2^-$ | 551.0 | $61/2^- \rightarrow 57/2^-$ | 5117.5 | $63/2^-$ | 541.6 | $63/2^- \rightarrow 59/2^-$ |
| 5407.5 | $65/2^-$ | 562.0 | $65/2^- \rightarrow 61/2^-$ | | | | |
| 5980.5 | $(69/2^-)$ | (573.0) | $(69/2^-) \rightarrow 65/2^-$ | | | | |
| | | Band 3 | | | | Band 4 | |
| 206.1 | $5/2^+$ | 206.1 | $5/2^+ \rightarrow 5/2^-$ | 235.2 | $7/2^+$ | 194.0 | $7/2^+ \rightarrow 7/2^-$ |
| | | 165.1 | $5/2^+ \rightarrow 7/2^-$ | | | | |
| 273.1 | $9/2^+$ | 179.5 | $9/2^+ \rightarrow 9/2^-$ | 320.2 | $11/2^+$ | | |
| 381.1 | $13/2^+$ | (108.0) | $13/2^+ \rightarrow 9/2^+$ | 453.5 | $15/2^+$ | 133.3 | $15/2^+ \rightarrow 11/2^+$ |
| | | 147.6 | $13/2^+ \rightarrow 13/2^-$ | | | | |
| 531.0 | $17/2^+$ | 149.9 | $17/2^+ \rightarrow 13/2^+$ | 630.2 | $19/2^+$ | 176.7 | $19/2^+ \rightarrow 15/2^+$ |
| | | 211.0 | $17/2^+ \rightarrow 15/2^-$ | | | | |
| 724.0 | $21/2^+$ | 193.0 | $21/2^+ \rightarrow 17/2^+$ | 851.7 | $23/2^+$ | 221.5 | $23/2^+ \rightarrow 19/2^+$ |
| | | 198.0 | $21/2^+ \rightarrow 19/2^-$ | | | 127.3 | $23/2^+ \rightarrow 21/2^+$ |
| 959.5 | $25/2^+$ | 235.5 | $25/2^+ \rightarrow 21/2^+$ | 1118.0 | $27/2^+$ | 266.3 | $27/2^+ \rightarrow 23/2^+$ |
| | | 185.6 | $25/2^+ \rightarrow 23/2^-$ | | | 158.2 | $27/2^+ \rightarrow 25/2^+$ |
| | | 108.1 | $25/2^+ \rightarrow 23/2^+$ | | | | |
| 1236.0 | $29/2^+$ | 276.5 | $29/2^+ \rightarrow 25/2^+$ | 1426.8 | $31/2^+$ | 308.8 | $31/2^+ \rightarrow 27/2^+$ |
| | | 174.3 | $29/2^+ \rightarrow 27/2^-$ | | | 190.5 | $31/2^+ \rightarrow 29/2^+$ |
| | | 118.3 | $29/2^+ \rightarrow 27/2^+$ | | | | |
| 1551.3 | $33/2^+$ | 315.3 | $33/2^+ \rightarrow 29/2^+$ | 1775.6 | $35/2^+$ | 348.8 | $35/2^+ \rightarrow 31/2^+$ |
| | | 124.8 | $33/2^+ \rightarrow 31/2^+$ | | | 224.0 | $35/2^+ \rightarrow 33/2^+$ |
| 1903.6 | $37/2^+$ | 352.3 | $37/2^+ \rightarrow 33/2^+$ | 2162.0 | $39/2^+$ | 386.4 | $39/2^+ \rightarrow 35/2^+$ |
| | | | | | | 258.1 | $39/2^+ \rightarrow 37/2^+$ |

TABLE II. (*Continued.*)

| $E_x$ (keV) | $J^\pi$ ($\hbar$) | $E_\gamma$ (keV) | Assignment | $E_x$ (keV) | $J^\pi$ ($\hbar$) | $E_\gamma$ (keV) | Assignment |
|---|---|---|---|---|---|---|---|
| | Band 3 | | | | Band 4 | | |
| 2289.8 | $41/2^+$ | 386.2 | $41/2^+ \rightarrow 37/2^+$ | 2583.1 | $43/2^+$ | 421.1 | $43/2^+ \rightarrow 39/2^+$ |
| 2708.1 | $45/2^+$ | 418.3 | $45/2^+ \rightarrow 41/2^+$ | 3036.7 | $47/2^+$ | 453.6 | $47/2^+ \rightarrow 43/2^+$ |
| 3156.8 | $49/2^+$ | 448.7 | $49/2^+ \rightarrow 45/2^+$ | 3521.2 | $51/2^+$ | 484.5 | $51/2^+ \rightarrow 47/2^+$ |
| 3633.6 | $53/2^+$ | 476.8 | $53/2^+ \rightarrow 49/2^+$ | 4034.8 | $55/2^+$ | 513.6 | $55/2^+ \rightarrow 51/2^+$ |
| 4137.7 | $57/2^+$ | 504.1 | $57/2^+ \rightarrow 53/2^+$ | 4577.6 | $(59/2^+)$ | (542.8) | $(59/2^+) \rightarrow 55/2^+$ |
| 4669.5 | $61/2^+$ | 531.8 | $61/2^+ \rightarrow 57/2^+$ | | | | |
| 5229.0 | $65/2^+$ | 559.5 | $65/2^+ \rightarrow 61/2^+$ | | | | |
| 5816.6 | $(69/2^+)$ | (587.6) | $(69/2^+) \rightarrow 65/2^+$ | | | | |
| | Band 5 | | | | Band 6 | | |
| 473.8 | $3/2^-$ | (472.0) | $3/2^- \rightarrow 5/2^-$ | 505.3 | $5/2^-$ | 505.3 | $5/2^- \rightarrow 5/2^-$ |
| 550.8 | $7/2^-$ | (77.0) | $7/2^- \rightarrow 3/2^-$ | 626.1 | $9/2^-$ | 120.8 | $9/2^- \rightarrow 5/2^-$ |
| | | 510.0 | $7/2^- \rightarrow 7/2^-$ | | | | |
| | | 455.9 | $7/2^- \rightarrow 9/2^-$ | | | | |
| 682.5 | $11/2^-$ | 131.7 | $11/2^- \rightarrow 7/2^-$ | 788.1 | $13/2^-$ | 162.0 | $13/2^- \rightarrow 9/2^-$ |
| | | | | | | (106.2) | $13/2^- \rightarrow 11/2^-$ |
| 864.2 | $15/2^-$ | 181.7 | $15/2^- \rightarrow 11/2^-$ | 990.0 | $17/2^-$ | 201.9 | $17/2^- \rightarrow 13/2^-$ |
| | | | | | | 124.5 | $17/2^- \rightarrow 15/2^-$ |
| 1085.7 | $19/2^-$ | 221.5 | $19/2^- \rightarrow 15/2^-$ | 1231.0 | $21/2^-$ | 241.0 | $21/2^- \rightarrow 17/2^-$ |
| | | (91.3) | $19/2^- \rightarrow 17/2^-$ | | | 147.2 | $21/2^- \rightarrow 19/2^-$ |
| 1346.0 | $23/2^-$ | 260.3 | $23/2^- \rightarrow 19/2^-$ | 1510.5 | $25/2^-$ | 279.5 | $25/2^- \rightarrow 21/2^-$ |
| | | (113.7) | $23/2^- \rightarrow 21/2^-$ | | | 164.9 | $25/2^- \rightarrow 23/2^-$ |
| 1643.8 | $27/2^-$ | 297.8 | $27/2^- \rightarrow 23/2^-$ | 1826.6 | $29/2^-$ | 316.1 | $29/2^- \rightarrow 25/2^-$ |
| | | 132.9 | $27/2^- \rightarrow 25/2^-$ | | | 184.5 | $29/2^- \rightarrow 27/2^-$ |
| 1977.4 | $31/2^-$ | 333.6 | $31/2^- \rightarrow 27/2^-$ | 2177.9 | $33/2^-$ | 351.3 | $33/2^- \rightarrow 29/2^-$ |
| | | 148.2 | $31/2^- \rightarrow 29/2^-$ | | | | |
| 2344.8 | $35/2^-$ | 367.8 | $35/2^- \rightarrow 31/2^-$ | 2561.4 | $37/2^-$ | 383.5 | $37/2^- \rightarrow 33/2^-$ |
| | | 166.2 | $35/2^- \rightarrow 33/2^-$ | | | | |
| 2744.7 | $39/2^-$ | 399.9 | $39/2^- \rightarrow 35/2^-$ | 2977.1 | $41/2^-$ | 415.7 | $41/2^- \rightarrow 37/2^-$ |
| 3175.6 | $43/2^-$ | 430.9 | $43/2^- \rightarrow 39/2^-$ | 3424.2 | $45/2^-$ | 447.1 | $45/2^- \rightarrow 41/2^-$ |
| 4636.0 | $47/2^-$ | 460.4 | $47/2^- \rightarrow 43/2^-$ | 3903.5 | $(49/2^-)$ | (479.3) | $(49/2^-) \rightarrow 45/2^-$ |
| 4123.4 | $51/2^-$ | 487.4 | $51/2^- \rightarrow 47/2^-$ | | | | |

where the top spectrum was obtained from the general coincidence cube used also to derive the structural information on $^{241}$Am, while the bottom one originates from a dedicated cube built with the requirement that either one of the two $^{208}$Pb transitions mentioned above is observed in Gammasphere. The yrast band of $^{242}$Cm is now established up to the $22^+$ level (see Fig. 8) from the observed coincidence relationships. A weak 488.6 keV $\gamma$ ray is tentatively proposed to deexcite the $24^+$ level. As stated above, several other reaction channels were observed in the measurements such as those involving one proton pickup leading to $^{240}$Pu, for example. The reader is referred to Ref. [19] for further details.

One proton pickup and transfer reactions leading to $^{236}$U and the $^{238}$Pu nuclei were observed with the $^{237}$Np target in addition to a number of channels involving the exchange of several nucleons. Among the latter, the one leading to $^{236}$Pu through the $^{237}$Np($^{209}$Bi, $^{210}$Pb) reaction is of interest here. The first eight $^{236}$Pu excited levels were originally established via the $^{235}$U$(\alpha, 3n)$ reaction by Hardt *et al.* [22]. Here, four additional $\gamma$ rays have been placed at the top of the cascade extending the ground state band to the $24^+$ state. The level scheme is presented together with that of $^{242}$Cm in Fig. 8. While this reaction channel is weak (of the order of 0.5% of the $^{237}$Np yield), as should be expected for such a complex reaction, there is little doubt about the assignment because of the observation of the entire cascade of Ref. [22], and the presence of both the characteristic Pu x rays and the 799.7 keV ground state transition in $^{210}$Pb in the coincidence spectra. Here too the reader is referred to Ref. [19] for further discussions and descriptions of other reaction channels.

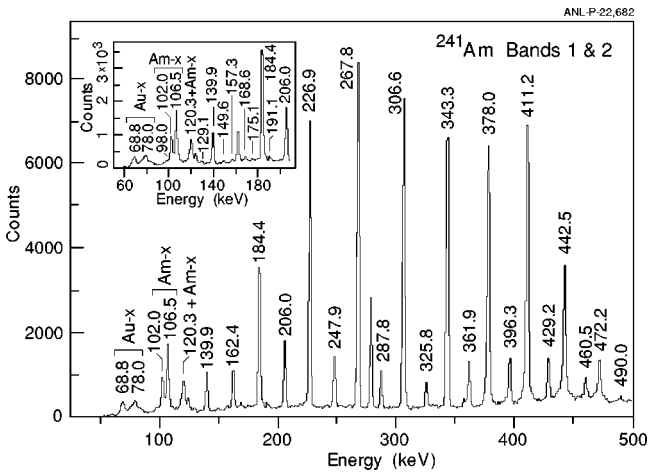


FIG. 5. Representative coincidence spectrum for bands 1 and 2 in $^{241}$Am. The spectrum has been obtained by summing over double coincidence gates placed on 139.9–378.0 keV sequence. The inset shows the low energy part of the spectrum in some detail.

## IV. DISCUSSION

One outstanding question associated with the high spin properties of the deformed actinides concerns the underlying configurations responsible for the alignment features observed in this region. Figure 9(a) presents alignment plots for the yrast bands of $^{232}$Th, $^{238}$U, and $^{244}$Pu, the isotope of each element observed to the highest spin. The Harris parameters $J_0 = 65\ \mathrm{MeV}^{-1}\hbar^2$ and $J_1 = 365\ \mathrm{MeV}^{-3}\hbar^4$, from Ref. [4], have been adopted. Each isotope experiences a substantial increase in alignment around $\hbar\omega \sim 0.25$ MeV. For the Th and U nuclei, where the increase in alignment with frequency is

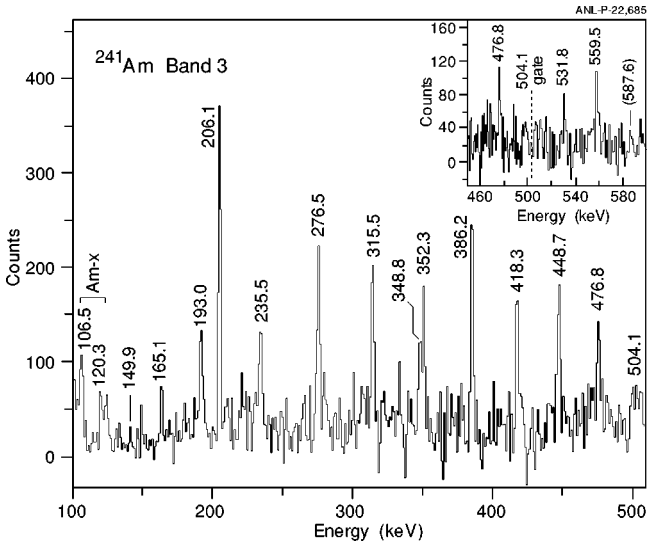


FIG. 6. Representative coincidence spectrum for band 3 in $^{241}$Am obtained by summing over selected double gates with one transition in the 235.5–386.2 keV cascade and the other in the 418.3–476.8 keV sequence. As described in the text, the inset displays the top of the band and is the result of a coincidence gate placed on the 504.1 keV line in coincidence with the 386.2–476.8 keV series.

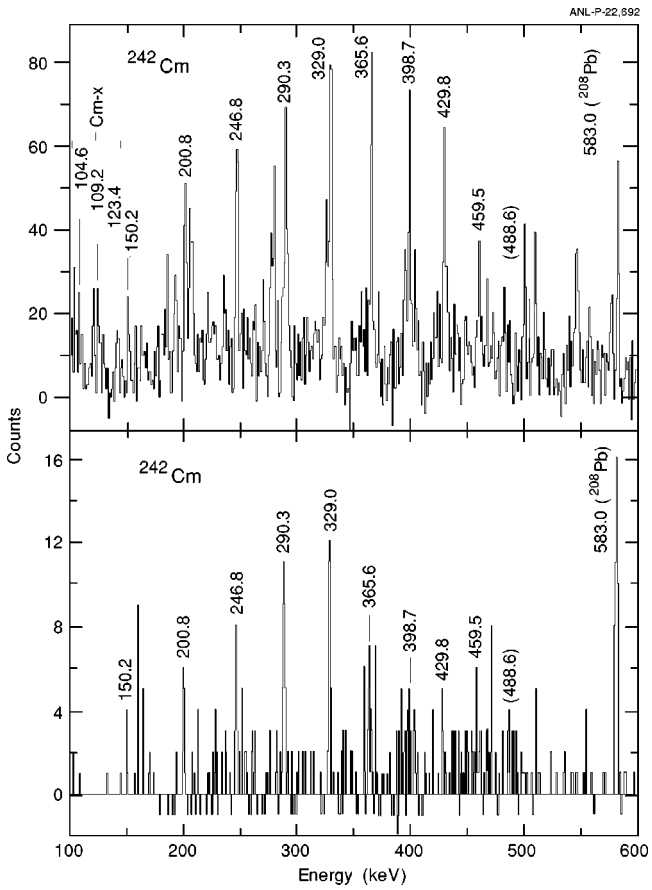


FIG. 7. Yrast band of $^{242}$Cm from the sum of spectra double gated on the 200.8–398.7 keV sequence in either the prompt coincidence cube (top), or in a dedicated coincidence cube updated only when either the 583 or 2614 keV transition from $^{208}$Pb are seen in Gammasphere (bottom), see text for details.

rather gradual, a number of authors have ascribed this rise to the near simultaneous alignment of $j_{15/2}$ neutron and $i_{13/2}$ proton pairs [2,3,12]. For the Pu isotopes, theoretical calculations attribute the more abrupt rise to an aligned pair of $i_{13/2}$ protons with a weak interaction at the crossing between paired and aligned configurations. However, the fact that the three bands in Fig. 9(a) gain roughly the same amount of alignment suggests that the same number of high-$j$ intruder pairs is involved in all three cases.

### A. Alignments in $^{237}$Np and $^{241}$Am

In order to determine which orbitals are responsible for an alignment, it is customary to invoke blocking arguments using high spin data from neighboring odd-A nuclei, where rotational bands built on high-$j$ intruder orbitals are observed, i.e., in this instance $i_{13/2}$ protons and $j_{15/2}$ neutrons. While high spin data have been available for some time for a number of even-even isotopes in this mass region, there are only a few good examples involving odd-A systems, most notably $^{235}$U and $^{237}$Np where bands built on these high-$j$ intruder orbitals have been delineated [15,23,24]. The present data provide the opportunity to study the issue further as the $i_{13/2}$ proton signature partner bands are extended

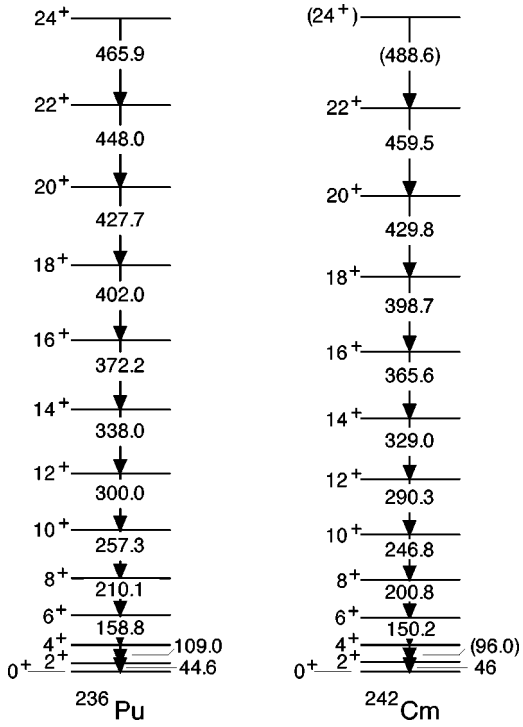


FIG. 8. Level schemes of $^{242}$Cm and $^{236}$Pu obtained in the present work.

to higher angular momentum and two bands built on the $h_{9/2}$ orbital are now established in $^{237}$Np. In the case of $^{241}$Am, the present work has delineated sequences built on $i_{13/2}$, $h_{9/2}$ and $f_{7/2}$ configurations over a large frequency range.

The bands built on the $i_{13/2}$ orbital are of particular interest since they "block" the first proton alignment and isolate the contribution of the $j_{15/2}$ neutrons. Figures 9(b) and 9(c) give the alignment curves for the $i_{13/2}$ and $h_{9/2}$ bands in $^{237}$Np and the $i_{13/2}$, $h_{9/2}$ and $f_{7/2}$ bands in $^{241}$Am. To facilitate the discussion, representative yrast bands of even-even neighbors are given as well. In both odd nuclei, the $i_{13/2}$ bands exhibit a nearly constant alignment while the even-even neighbors experience upbends in their alignment plots. Furthermore, in $^{237}$Np, both signatures of the $h_{9/2}$ band show the same alignment gain as observed in $^{236}$U, i.e., a gradual gain with frequency indicative of a strong interaction between the aligned and paired configurations. In $^{241}$Am, both signatures of the $h_{9/2}$ band show the beginnings of a sharp upbend at $\hbar\omega \sim 0.26$ MeV which mimics that observed in $^{242}$Pu. The absence of an upbend in the two signatures of the $f_{7/2}$ band is not surprising as they do not reach sufficiently high in rotational frequency to experience the expected alignment. The constant alignment in the $i_{13/2}$ bands, and the striking similarity between the behaviors of the $h_{9/2}$ bands and the yrast bands of the even-even neighbors indicate that the $i_{13/2}$ protons are solely responsible for the upbends observed in both the U and Pu isotopes. In addition, the alignment contributions from the two $i_{13/2}$ signature partners in $^{237}$Np and $^{241}$Am add up to $\sim 7-8\hbar$, approximating the total alignment gain observed in the even-even yrast bands. This leaves little room for alignment contributions from a $j_{15/2}$ quasineutron pair, lending further support to this interpretation.

New high spin data have also become available recently for $^{235}$U [24], complementing the earlier results of Ref. [23]. Three pairs of rotational bands, one assigned to the $j_{15/2}$ neutron intruder configuration and two associated with the natural parity orbitals $[631]1/2^+$ $(3d_{5/2})$ and $[622]5/2^+$ $(1i_{11/2})$, are compared in terms of their alignments with the yrast band of $^{236}$U in Fig. 9(d). Unlike the marked difference in alignment noted for the $i_{13/2}$ proton bands in

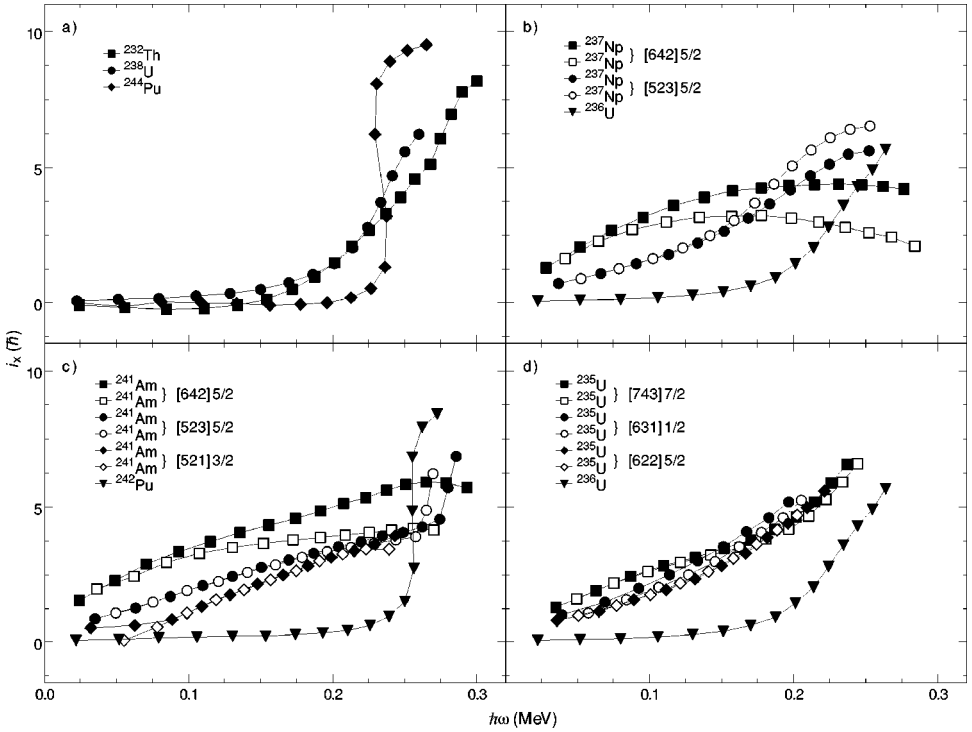


FIG. 9. Alignments as a function of rotational frequency for: (a) representative even actinide nuclei $^{232}$Th, $^{238}$U and $^{244}$Pu; (b) the $^{237}$Np bands delineated in this work compared with the yrast sequence of $^{236}$U; (c) the three pairs of rotational cascades found in $^{241}$Am together with the yrast band of $^{242}$Pu; (d) three bands of $^{235}$U compared with the neighboring even $^{236}$U nucleus. See text for details.

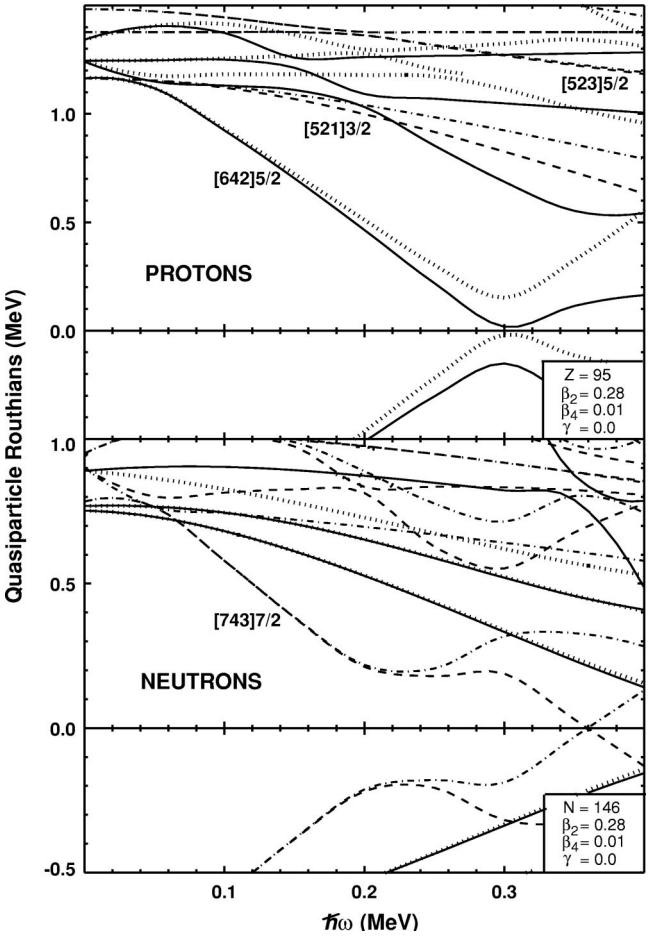


FIG. 10. Sample results of CSM calculations for protons and neutrons in $^{241}$Am. The labels for the configurations of interest are located just below the actual Routhians. See text for further details.

$^{241}$Am and $^{237}$Np, the evolution of the $j_{15/2}$ band with rotational frequency in $^{235}$U is quite similar to that of the other two pairs of rotational bands: all six bands experience a band crossing at $\hbar\omega \sim 0.2$ MeV which is due to $i_{13/2}$ protons, and the rise with frequency is of comparable magnitude. This similarity of the alignment behavior for all the bands leaves little room for a $j_{15/2}$ neutron alignment. This conclusion is consistent with the interpretation of the $^{237}$Np and $^{241}$Am data presented above.

The available experimental information indicates clearly that the $j_{15/2}$ neutrons do not play a major role in the observed backbending behavior of the actinide nuclei. A similar conclusion was reached in Ref. [15] where it was speculated that the expected neutron crossing must be located higher in rotational frequency, outside the range covered by the measurements, and/or must be associated with a very weak interaction. Figure 10 provides the results of standard cranked shell model (CSM) calculations with the Warsaw–Lund code which uses a Woods–Saxon potential [25] with the universal parameters given in Ref. [26]. These calculations predict that the $j_{15/2}$ neutrons should align around $\hbar\omega \sim 0.22$ MeV and that this alignment should be followed by the $i_{13/2}$ proton crossing at $\hbar\omega \sim 0.30$ MeV, in clear contradiction with the conclusions reached from the experimental data. A variation within realistic limits of the deformation parameters $\beta_2$ (0.25−0.3) and $\beta_4$ (0.0−0.04) is unable to change the crossing frequency of either the neutrons or protons by more than 0.02 MeV. The $i_{13/2}$ proton crossing can be lowered below 0.25 MeV by decreasing the pairing strength, $G$, by 10−15%. A similar reduction in the pairing strength for the neutrons also lowers the associated crossing frequency for the $j_{15/2}$ quasineutron alignment to $\hbar\omega \sim 0.15$ MeV. However, the remaining neutron pair gap $\Delta$ is only 0.5 MeV in this case. With such little pairing, it is likely that the $j_{15/2}$ neutrons would slowly align with rotational frequency rather than decouple at a critical frequency as the protons do. If this were to be the case, major changes in the alignment plots would not be expected or observed.

This interpretation depends on a seemingly unjustifiable decrease in the pairing strength used in the model. Interestingly, it should be noted that a similar reduction in pairing strength was introduced in cranked relativistic mean field calculations performed to reproduce the moments of inertia observed in the yrast bands of $^{252,254}$No ($Z=102$, and $N=150,152$) [11]. The reason for the reduction in pairing strength in these calculations is not yet understood, but is consistent with the present suggestion of a weaker than expected pairing in the U-Pu nuclei. Another possible explanation might invoke the formulation of the pairing force itself, i.e., its density dependence, as discussed in Ref. [10].

### B. Experimental Routhians

Another aspect of the data to be compared to CSM calculations is the experimental single-particle Routhians. Figure 11 shows these quantities as a function of rotational frequency for the bands in $^{237}$Np and $^{241}$Am. Also included in the $^{237}$Np panel are the first few levels assigned to the $[521]3/2^-$ configuration from decay work [14]. With regards to signature splitting, the experimental data and CSM calculations compare rather well. In both nuclei, the $[642]5/2^+$ bands exhibit a splitting which increases gradually with frequency as predicted by the calculations (Fig. 10). Conversely, no signature splitting occurs in the $[523]5/2^-$ bands before the first band crossing, again in agreement with the calculations. Finally, the $[521]3/2^-$ bands in $^{241}$Am experience signature splitting over the entire frequency range, matching the behavior of this orbital in the CSM calculations (Fig. 10). All these observations lend support to the proposed single-particle assignments. In contrast, the ordering in absolute energy of the $[523]5/2^-$ and $[521]3/2^-$ configurations is not in agreement with the CSM. Both in $^{237}$Np and $^{241}$Am, the $[521]3/2^-$ bands are predicted to lie lower in energy than the $[523]5/2^-$ bands while the experimental ordering is reversed. This observation points to a problem in calculating the relative positions of the $h_{9/2}$ and $f_{7/2}$ orbitals using the parametrization of the Woods–Saxon potential of Ref. [26].

### C. Alignments in $^{242}$Cm and $^{236}$Pu

As stated above, the alignments observed in the even-even Pu isotopes have been a matter of interest mostly be-

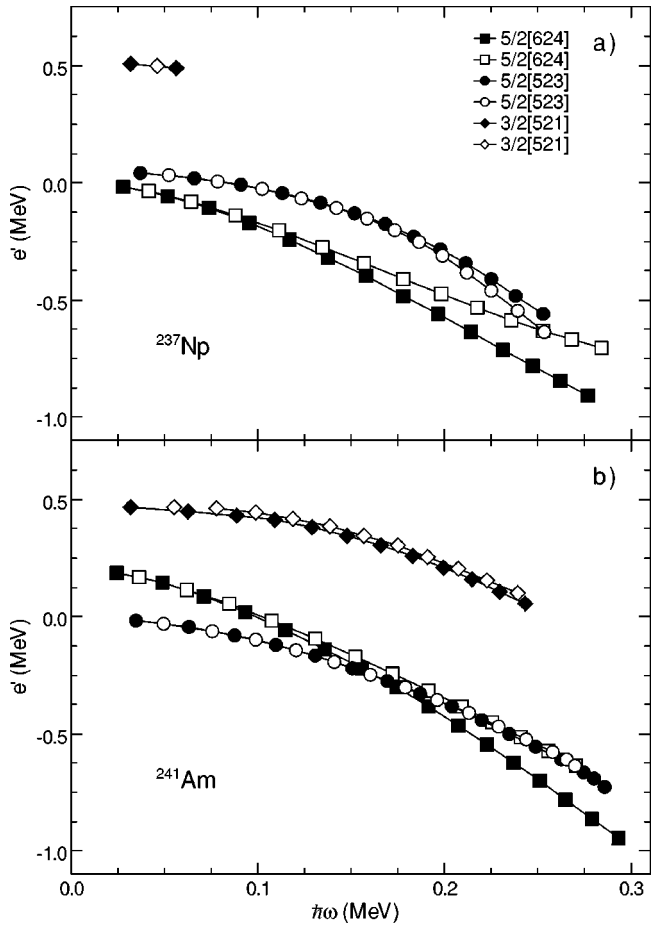


FIG. 11. Routhians for the band structures observed in $^{237}$Np and $^{241}$Am. Defined as $e'(\omega)=E-\omega I_x(\omega)-E'_g(\omega)+\Delta_{o-e}$ where $E$ is the excitation energy, $\Delta$ is related to the odd-even mass difference, and $E'_g$ represents the energy of the core in the rotating frame. $E'_g$ is defined as $E'(\omega)=-(\omega^2/2)J_0-(\omega^4/4)J_1+1/8J_0$ where $J_0$ and $J_1$ are the Harris parameters given in the text.

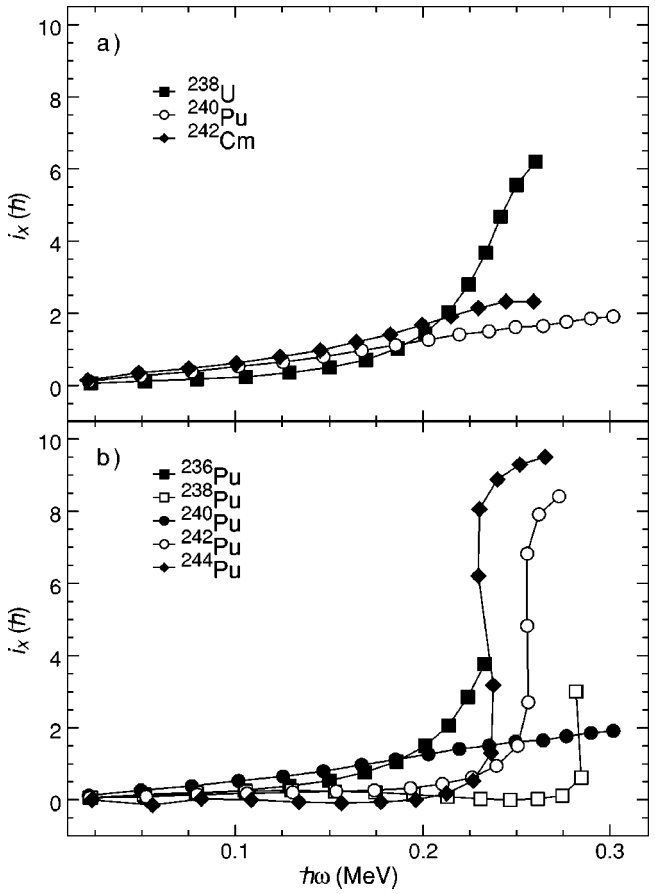


FIG. 12. Alignments as a function of rotational frequency for (a) the $N=146$ U, Pu and Cm isotones, and (b) for all known even Pu isotopes with $A=236-244$.

cause of the fact that the sharp backbending observed in the heavier isotopes is not present within the same frequency range in the lighter $^{238,239,240}$Pu, implying at the minimum a significant delay in the alignment process [4]. The data obtained in the present measurements shed additional light on this issue. Figure 12(a) compares as a function of the rotational frequency the alignments observed in the yrast bands of the three $N=146$ isotones $^{238}$U, $^{240}$Pu and $^{242}$Cm. The alignment pattern for $^{242}$Cm mirrors that seen in $^{240}$Pu: in both nuclei there is a small rise in alignment with frequency ($\Delta i \leqslant 2\hbar$) and there is no sign of a sudden increase around $\hbar\omega=0.25$ MeV where $^{238}$U and the heavier even-even Pu isotopes align. In contrast, Fig. 12(b) indicates that $^{236}$Pu gains considerable alignment within the frequency range of interest, but that this alignment is somewhat more gradual than in the heaviest Pu isotopes. Thus, the region where the $i_{13/2}$ proton alignment is either delayed or absent extends only to the three Pu isotopes with $A=238-240$. It is worth noting that, while the frequency range where this difference in alignment pattern occurs may appear insignificant at first sight, it represents a difference in behavior extending over at least $5-6$ $\gamma$ rays in the respective yrast sequences. Furthermore, the absence of alignment in the Cm isotopes is likely to be limited to rather few nuclei as well since $^{246}$Cm and $^{248}$Cm exhibit alignment patterns similar to those seen in the heavier Pu isotopes [19,27].

Within the framework of the CSM, as well as on the basis of considerations in terms of blocking presented above, the alignment behaviors of $^{238,240}$Pu and $^{242}$Cm are quite surprising. Since these alignments can be ascribed to $i_{13/2}$ protons in the heavier Pu and Cm nuclei, and since the deformations of all these nuclei are essentially the same, there is no *a priori* reason for any marked difference. This statement is corroborated by CSM calculations which predict comparable crossing frequencies and alignments for all the isotopes under consideration [19]. It was argued in Ref. [4] that the absence and/or the delay in the frequency could be due to octupole deformation effects. As shown in the latter work, only in $^{238-240}$Pu do the states of the yrast band become interleaved at high spin with levels of negative parity to the extent that they essentially form a single band as in $^{222}$Th and $^{229}$Ra [28], two of the best examples of nuclei with octupole deformation. Also, in $^{239}$Pu, states with the same spin, but opposite parity, are located close in energy and appear to form so-called parity doublets, as would be expected for odd nuclei with octupole deformation. Additional evidence is provided

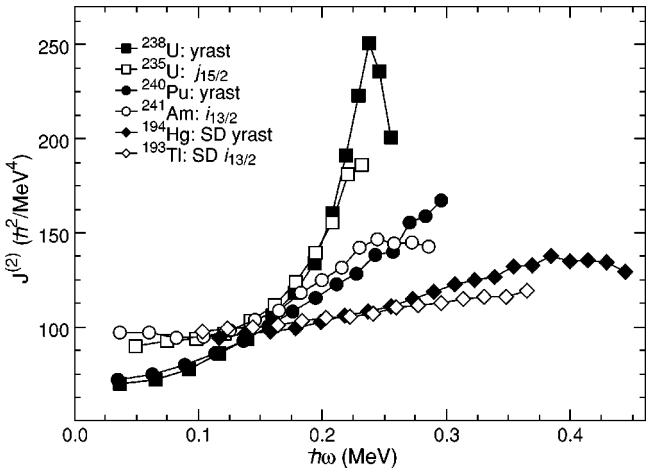


FIG. 13. Dynamic moments of inertia $J^{(2)}$ as a function of rotational frequency for selected bands discussed in the text.

by the measured ratios of the reduced $E1$ and $E2$ transition rates: the values of the induced intrinsic dipole moment deduced from such data become quite large at high spin only in $^{238-240}$Pu. Finally, as discussed by Sheline and Riley [5], the hindrance factors for alpha decay in the light Pu isotopes are smaller than those seen in all neighboring nuclei and are of the same order as the values measured in the octupole deformed Ra, Rn, and Th nuclei. From this point of view the present data then serve to indicate that these octupole correlations play a major role only in a very limited region, as $^{236}$Pu indicates a return to the more usual alignment pattern.

### D. Dynamic moments of inertia: Search for traces of a $\nu j_{15/2}$ alignment

While a coherent picture appears to emerge from the discussion above, one remaining question relates to whether or not any fingerprint of a $j_{15/2}$ neutron alignment can be found in the available experimental data on actinide nuclei. The dynamic moments of inertia, $J^{(2)}$, are presented in Fig. 13 as a function of rotational frequency for the yrast bands of $^{238}$U and $^{240}$Pu, the $i_{13/2}$ proton band in $^{241}$Am, the $j_{15/2}$ neutron band in $^{235}$U, the yrast superdeformed (SD) band in $^{194}$Hg [29] and a SD band built on the $i_{13/2}$ proton orbital in $^{193}$Tl [30]. This $J^{(2)}$ moment is inversely proportional to the energy difference between consecutive transitions in a rotational band and is independent of spin, i.e., $J^{(2)} \sim 4/\Delta E_\gamma$. The largest increase in the $J^{(2)}$ moment occurs for $^{238}$U and $^{235}$U, and this rise can be attributed straightforwardly to the $i_{13/2}$ proton alignment discussed above. (This large increase in the $J^{(2)}$ moment is indicative of all bands in the region which experience the $\pi i_{13/2}$ band crossing). In addition, even though the moments of inertia of these two bands deviate from each other at low frequency, they become nearly identical once the alignment begins. For the cases of $^{240}$Pu and the $i_{13/2}$ band of $^{241}$Am, the proton alignment is not observed. However, the two bands also behave in a similar manner, i.e., at low frequency their moments of inertia deviate from each other, but above $\hbar\omega = 0.125$ MeV, their $J^{(2)}$ behavior is similar. At the highest frequencies, the rise in the $J^{(2)}$ moment levels off in $^{241}$Am. It is worth noting that the behavior of the $i_{13/2}$ band in $^{237}$Np (not shown) tracks that of the yrast band in $^{240}$Pu and the $i_{13/2}$ band of $^{241}$Am.

Within the CSM, the interpretation that the lack of backbending features associated with $j_{15/2}$ neutrons is a consequence of reduced pairing for these actinide nuclei is similar to the generally accepted description of the alignments of $i_{13/2}$ proton and $j_{15/2}$ neutron pairs in the $A \sim 190$ superdeformed (SD) region [29]. The dynamic moments of inertia of nearly all SD bands in this mass region increase smoothly with rotational frequency as is illustrated by the two SD bands of Fig. 13. However, a careful analysis of the $J^{(2)}$ moments of these SD bands clearly shows that a portion of this rise is brought about by the gradual alignment of both $j_{15/2}$ neutrons and $i_{13/2}$ protons [31] and the individual contributions can be disentangled [6,31]. In the case of $^{194}$Hg, the leveling off of the $J^{(2)}$ moment at the highest frequencies has been cited as strong evidence that this interpretation is correct and the nearly constant $J^{(2)}$ moment results from the fact that, at the highest $\hbar\omega$ values, both proton and neutron intruder configurations are essentially aligned with the rotational axis [29]. Thus, in analogy, it is probable that a portion of the modest rise in $J^{(2)}$ observed for both $^{240}$Pu and $^{241}$Am in Fig. 13 is due to the gradual alignment of $j_{15/2}$ neutrons. It then follows that the leveling off of the $J^{(2)}$ moment in $^{241}$Am is due to the near alignment of the $j_{15/2}$ neutrons with the rotational axis, while the corresponding $J^{(2)}$ moment continues to rise in $^{240}$Pu, which may indicate the onset of a delayed $i_{13/2}$ proton alignment. This interpretation, if correct, also indicates that in $^{240}$Pu only the proton alignment is delayed and the neutrons behave in a manner similar to that seen in the neighboring isotopes.

Finally, it is also interesting to note that the moments of inertia of the SD bands are very similar in magnitude to those of the actinide rotational bands at the lower frequencies, even though the quadrupole deformations are quite different. This is due to the fact that these $J^{(2)}$ moments are largely dependent on the valence orbitals, and in particular, on the high-$j$ intruder configurations [32]. As pointed out above, for both the SD and actinide bands, the dominant intruder orbitals are the $j_{15/2}$ neutrons and $i_{13/2}$ protons. The deviations between moments at larger frequencies are then due mainly to how these same intruder orbitals align under the stress of rotation in differing deformation regimes.

## V. CONCLUSIONS

The level structures of the odd-proton actinide nuclei $^{237}$Np and $^{241}$Am have been considerably extended in a set of experiments using the "unsafe" Coulomb excitation technique. As a result, outstanding issues related to the $i_{13/2}$ proton and $j_{15/2}$ neutron alignments in the actinide region could be investigated in some detail. Blocking arguments were used to designate $i_{13/2}$ protons as the major contributors to the smooth upbending seen in the Th and U even-even nuclei and to the backbending observed in the heaviest Pu isotopes.

Cranked shell model calculations can reproduce the main experimental observations only if a reduction of 10–15% in the pairing strength is assumed. While a microscopic justification for such a reduction is at present lacking, it was shown that, under such a scenario, the measured crossing frequencies as well as the lack of a strong $j_{15/2}$ neutron contribution to the alignment can be accounted for. Similarities between the present situation and that observed in superdeformed nuclei of the $A\sim190$ region were highlighted. Finally, data obtained on the even nuclei $^{242}$Cm and $^{236}$Pu from transfer reactions were instrumental in exploring further the striking difference in the alignment pattern with frequency of $^{238-240}$Pu when compared to the other Pu nuclei.

## ACKNOWLEDGMENTS

Stimulating discussions with A. Afanasjev, T. Duguet, L. Egido, S. Frauendorf, F. Iachello, P.-H. Heenen, W. Nazarewicz and T. Nakatsukasa are gratefully acknowledged. This work is supported by the U.S. Department of Energy, Office of Nuclear Physics, under Contract Nos. W–31–109–ENG–38, DE–FG02–94ER40848, DE–FG03–96ER40981, DE–AC03–76SF00098, W–7405–ENG–36 and by the National Science Foundation. The authors are indebted for the use of Np and Am isotopes to the office of Basic Energy Sciences, U.S. Department of Energy, through the transplutonium element production facilities at the Oak Ridge National Laboratory.

[1] W. Spreng, F. Azgui, H. Emling, E. Grosse, R. Kulessa, Ch. Michel, D. Schwalm, R. S. Simon, H. J. Wollersheim, M. Mutterer, J. P. Theobald, M. S. Moore, N. Trautmann, J. L. Egido, and P. Ring, Phys. Rev. Lett. **51**, 1522 (1983).

[2] J. Dudek, W. Nazarewicz, and Z. Szymanski, Phys. Scr. **T5**, 171 (1983), and references therein.

[3] J. L. Egido and P. Ring, Nucl. Phys. **A423**, 93 (1984).

[4] I. Wiedenhöver, R. V. F. Janssens, G. Hackman, I. Ahmad, J. P. Greene, H. Amro, P. K. Bhattacharyya, M. P. Carpenter, P. Chowdhury, J. Cizewski, D. Cline, T. L. Khoo, T. Lauritsen, C. J. Lister, A. O. Macchiavelli, D. T. Nisius, P. Reiter, E. H. Seabury, D. Seweryniak, S. Siem, A. Sonzogni, J. Uusitalo, and C. Y. Wu, Phys. Rev. Lett. **83**, 2143 (1999).

[5] R. K. Sheline and M. A. Riley, Phys. Rev. C **61**, 057301 (2000).

[6] R. V. F. Janssens and T. L. Khoo, Annu. Rev. Nucl. Part. Sci. **41**, 321 (1991).

[7] B. Crowell, M. P. Carpenter, R. V. F. Janssens, D. J. Blumenthal, J. Timar, A. N. Wilson, J. F. Sharpey-Schafer, T. Nakatsukasa, I. Ahmad, A. Astier, F. Azaiez, L. du Croux, B. J. P. Gall, F. Hannachi, T. L. Khoo, A. Korichi, T. Lauritsen, A. Lopez-Martens, M. Meyer, D. Nisius, E. S. Paul, M. G. Porquet, and N. Redon, Phys. Rev. C **51**, R1599 (1995); A. N. Wilson, J. Timar, J. F. Sharpey-Schafer, B. Crowell, M. P. Carpenter, R. V. F. Janssens, D. J. Blumenthal, I. Ahmad, A. Astier, F. Azaiez, M. Bergstrom, L. Ducroux, B. J. P. Gall, F. Hannachi, T. L. Khoo, A. Korichi, T. Lauritsen, A. Lopez-Martens, M. Meyer, D. Nisius, E. S. Paul, M. G. Porquet, N. Redon, J. N. Wilson, and T. Nakatsukasa, Phys. Rev. C **54**, 559 (1996); H. Amro, E. F. Moore, R. V. F. Janssens, G. Hackman, S. M. Fischer, M. P. Carpenter, I. Ahmad, B. Crowell, T. L. Khoo, T. Lauritsen, D. Nisius, J. Timar, and A. N. Wilson, Phys. Lett. B **413**, 15 (1997).

[8] G. Hackman, T. L. Khoo, M. P. Carpenter, T. Lauritsen, A. Lopez-Martens, I. J. Calderin, R. V. F. Janssens, D. Ackermann, I. Ahmad, S. Agarwala, D. J. Blumenthal, S. M. Fischer, D. Nisius, P. Reiter, J. Young, H. Amro, E. F. Moore, F. Hannachi, A. Korichi, I. Y. Lee, A. O. Macchiavelli, T. Døssing, and T. Nakatsukasa, Phys. Rev. Lett. **79**, 4100 (1997); S. Bouneau, F. Azaiez, J. Duprat, I. Deloncle, M.-G. Porquet, U. J. van Severen, T. Nakatsukasa, M.-M. Aleonard, A. Astier, G. Baldsiefen, C. W. Beausang, F. A. Beck, C. Bourgeois, D. Curien, N. Dozie, L. Ducroux, B. J. P. Gall, H. Hubel, M. Kaci, W. Korten, M. Meyer, N. Redon, H. Sergolle, and J. F. Sharpey-Schafer, Z. Phys. A **358**, 179 (1997).

[9] P. Reiter, T. L. Khoo, C. J. Lister, D. Seweryniak, I. Ahmad, M. Alcorta, M. P. Carpenter, J. Cizewski, C. N. Davids, G. Gervais, J. P. Greene, W. F. Henning, R. V. F. Janssens, T. Lauritsen, S. Siem, A. A. Sonzogni, D. Sullivan, J. Uusitalo, I. Wiedenhöver, N. Amzal, P. A. Butler, A. J. Chewter, K. Y. Ding, N. Fotiades, J. D. Fox, P. T. Greenless, R.-D. Herzberg, G. D. Jones, W. Korten, M. Leino, and K. Vetter, Phys. Rev. Lett. **82**, 509 (1999); M. Leino, H. Kankaanpää, R.-D. Herzberg, A. J. Chewter, F. P. Heßberger, Y. Le Coz, F. Becker, P. A. Butler, J. F. C. Cocks, O. Dorvaux, K. Eskola, J. Gerl, P. T. Greenless, K. Helariutta, M. Houry, G. D. Jones, P. Jones, R. Julin, S. Juutinen, H. Kettunen, T. L. Khoo, A. Kleinbohl, W. Korten, P. Kuusiniemi, R. Lucas, M. Muikku, P. Nieminen, R. D. Page, P. Rahkila, P. Reiter, A. Savelius, Ch. Schlegel, Ch. Theisen, W. H. Trzaska, and H.-J. Wollersheim, Eur. Phys. J. A **6**, 63 (1999); P. Reiter, T. L. Khoo, T. Lauritsen, C. J. Lister, D. Seweryniak, A. A. Sonzogni, I. Ahmad, N. Amzal, P. Bhattacharyya, P. A. Butler, M. P. Carpenter, A. J. Chewter, J. A. Cizewski, C. N. Davids, K. Y. Ding, N. Fotiades, J. P. Greene, P. T. Greenless, A. Heinz, W. F. Henning, R.-D. Herzberg, R. V. F. Janssens, G. D. Jones, H. Kankaanpää, F. G. Kondev, W. Korten, M. Leino, S. Siem, J. Uusitalo, K. Vetter, and I. Wiedenhöver, Phys. Rev. Lett. **84**, 3542 (2000); R.-D. Herzberg, N. Amzal, F. Becker, P. A. Butler, A. J. Chewter, J. F. C. Cocks, O. Dorvaux, K. Eskola, J. Gerl, P. T. Greenless, N. J. Hammond, K. Hauschild, K. Helariutta, F. P. Heßberger, M. Houry, G. D. Jones, P. M. Jones, R. Julin, S. Juutinen, H. Kankaanpää, H. Kettunen, T. L. Khoo, W. Korten, P. Kuusiniemi, Y. Le Coz, M. Leino, C. J. Lister, R. Lucas, M. Muikku, P. Nieminen, R. D. Page, P. Rahkila, P. Reiter, Ch. Schlegel, C. Scholey, O. Stezowski, Ch. Theisen, W. H. Trzaska, J. Uusitalo, and H.-J. Wollersheim, Phys. Rev. C **65**, 014303 (2002).

[10] T. Duguet, P. Bonche, and P.-H. Heenen, Nucl. Phys. **A679**, 427 (2001); M. Bender, P. Bonche, T. Duguet, and P.-H. Heenen, Nucl. Phys. **A723**, 354 (2003).

[11] A. V. Afanasjev, T. L. Khoo, S. Frauendorf, G. A. Lalazissis,

and I. Ahmad, Phys. Rev. C **67**, 024309 (2003).
[12] D. Ward, H. R. Andrews, G. C. Ball, A. Galindo-Uribarri, V. P. Janzen, T. Nakatsukasa, D. C. Radford, T. E. Drake, J. DeGraaf, S. Pilotte, and Y. R. Shimizu, Nucl. Phys. **A600**, 88 (1996).
[13] Y. A. Akovali, Nucl. Data Sheets **72**, 191 (1994).
[14] Y. A. Akovali, Nucl. Data Sheets **74**, 461 (1995).
[15] R. Kulessa, R. P. DeVito, H. Emling, E. Grosse, D. Schwalm, R. S. Simon, A. Lefebvre, Ch. Briancon, R. J. Walen, G. Sletten, and Th. W. Elze, Z. Phys. A **312**, 135 (1983).
[16] J. P. Greene, R. V. F. Janssens, and I. Ahmad, Nucl. Instrum. Methods Phys. Res. A **438**, 119 (1999).
[17] I. Y. Lee, Nucl. Phys. **A520**, 641c (1990).
[18] D. C. Radford, Nucl. Instrum. Methods Phys. Res. A **361**, 306 (1995).
[19] K. Abu Saleem, Ph.D. thesis, Illinois Institute of Technology, 2002.
[20] Measured relative intensities can be found in Ref. [19]. Many of the transitions involved here are of low energy, where uncertainties are rather large because of poor Ge timing. While the measured values are sufficient to validate the level schemes presented here, they are not of a quality suitable for the extraction of branching ratios with the desired accuracy.
[21] Y. A. Akovali, Nucl. Data Sheets **96**, 177 (2002).
[22] K. Hardt, P. Schüler, C. Günther, J. Recht, and K. P. Blume, Nucl. Phys. **A407**, 127 (1983).
[23] J. de Bettencourt, Ch. Briancon, J. Libert, J. P. Thibaud, R. J. Walen, A. Gizon, M. Meyer, and Ph. Quentin, Phys. Rev. C **34**, 1706 (1986).
[24] D. Ward *et al.* (to be published).
[25] W. Nazarewicz, J. Dudek, R. Bengtsson, T. Bengtsson, and I. Ragnarsson, Nucl. Phys. **A435**, 397 (1985).
[26] J. Dudek, Z. Szymanski, and T. Werner, Phys. Rev. C **23**, 920 (1981).
[27] G. Hackman, R. V. F. Janssens, T. L. Khoo, I. Ahmad, J. P. Greene, H. Amro, D. Ackermann, M. P. Carpenter, S. M. Fischer, T. Lauritsen, L. R. Morss, P. Reiter, D. Seweryniak, D. Cline, C. Y. Wu, E. F. Moore, and T. Nakatsukasa, Phys. Rev. C **57**, R1056 (1998).
[28] P. A. Butler and W. Nazarewicz, Rev. Mod. Phys. **68**, 349 (1996).
[29] B. Cederwall, R. V. F. Janssens, M. J. Brinkman, I. Y. Lee, I. Ahmad, J. A. Becker, M. P. Carpenter, B. Crowell, M. A. Deleplanque, R. M. Diamond, J. E. Draper, C. Duyar, P. Fallon, L. P. Farris, E. A. Henry, R. G. Henry, J. R. Hughes, T. L. Khoo, T. Lauritsen, A. O. Macchiavelli, E. Rubel, F. S. Stephens, M. A. Stoyer, W. Satula, I. Wiedenhoever, and R. Wyss, Phys. Rev. Lett. **72**, 3150 (1994).
[30] S. Bouneau, F. Azaiez, J. Duprat, I. Deloncle, M. G. Porquet, A. Astier, M. Bergström, C. Bourgeois, L. Ducroux, B. J. P. Gall, M. Kaci, Y. Le Coz, M. Meyer, E. S. Paul, N. Redon, M. A. Riley, H. Sergolle, J. F. Sharpey-Schafer, J. Timar, A. N. Wilson, R. Wyss, and P.-H. Heenen, Phys. Rev. C **58**, 3260 (1998).
[31] D. Ye, R. V. F. Janssens, M. P. Carpenter, E. F. Moore, R. R. Chasman, I. Ahmad, K. B. Beard, Ph. Benet, M. W. Drigert, P. B. Fernandez, U. Garg, T. L. Khoo, S. L. Ridley, and F. L. H. Wolfs, Phys. Rev. C **41**, R13 (1990).
[32] T. Bengtsson, I. Ragnarsson, and S. Åberg, Phys. Lett. B **208**, 39 (1988).